

Attack Agnostic Detection of Adversarial Examples via Random Subspace Analysis

Nathan Drenkow, Neil Fendley, Philippe Burlina
The Johns Hopkins University Applied Physics Laboratory
Laurel, MD 20723, USA
{first.last}@jhuapl.edu

Abstract

Whilst adversarial attack detection has received considerable attention, it remains a fundamentally challenging problem from two perspectives. First, while threat models can be well-defined, attacker strategies may still vary widely within those constraints. Therefore, detection should be considered as an open-set problem, standing in contrast to most current detection approaches. These methods take a closed-set view and train binary detectors, thus biasing detection toward attacks seen during detector training. Second, limited information is available at test time and typically confounded by nuisance factors including the label and underlying content of the image. We address these challenges via a novel strategy based on random subspace analysis. We present a technique that utilizes properties of random projections to characterize the behavior of clean and adversarial examples across a diverse set of subspaces. The self-consistency (or inconsistency) of model activations is leveraged to discern clean from adversarial examples. Performance evaluations demonstrate that our technique ($AUC \in [0.92, 0.98]$) outperforms competing detection strategies ($AUC \in [0.30, 0.79]$), while remaining truly agnostic to the attack strategy (for both targeted/untargeted attacks). It also requires significantly less calibration data (composed only of clean examples) than competing approaches to achieve this performance.

1. Introduction

The rise of deep learning has led to state-of-the-art advances in machine learning (ML) across almost every conceivable application. With deep neural networks (DNNs) as the core computational elements in increasingly complex ML systems, there is greater demand for increasing DNN robustness to adversarial attacks.

The discovery of adversarial examples [16] has led to a wide range of subsequent findings in domains such as image classification, object detection, natural language process-

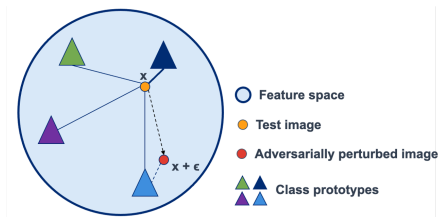


Figure 1. Distances in feature space between an image embedding (x) and class prototypes are used as a proxy for predicting class labels. Adversarial perturbations (ϵ) shift the clean representation such that the distance to the true class prototype increases and the distance to the incorrect prototype decreases.

ing, speech processing, and reinforcement learning. While adversarial examples are realized in the input domain, their intended and ultimate effect is on model behavior. To mitigate against potential attacks, we develop a model-centric, attack-agnostic method for adversarial example (AE) detection which analyzes the consistency of model activations under random projections. Our detection method is successful for a variety of attack strategies (e.g., FGSM [16], PGD [37], CWL [6]) and targeted/untargeted attacks. Our approach requires a small amount of calibration data and no *a priori* attack-specific knowledge or data.

2. Related Work

While developing novel attack and defense strategies occupies a large proportion of current and past AML research work, interest in automated detection of adversarial examples has grown considerably in recent years. Adversarial detection is a complementary problem to adversarial defense, but we focus here on efforts to explicitly predict cases of adversarial manipulation and leave it to downstream methods to mitigate the effects of any such manipulations.

We find the bulk of the AE detection work falls roughly into the following categories:

- **Input-space detection** - Methods that seek to

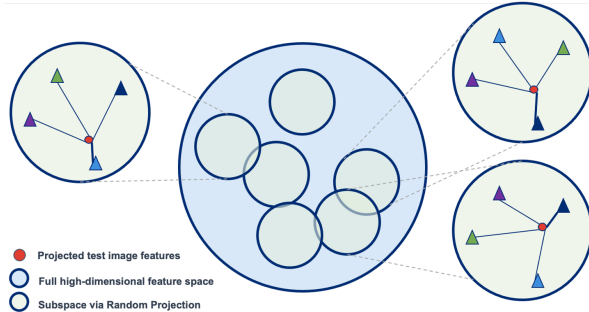


Figure 2. *Adversarial example detection via Random Subspace Analysis.* Random projections provide a mechanism for studying activation behavior with the aim to detect clean vs. adversarial examples. The likely existence of *non-robust but useful features* is exploited by measuring the consistency of the activation and latent space properties across multiple subspaces. Shown above, the two subspaces on the right are consistent with respect to which class prototype (colored triangles) is closest to the test point (red circle). The leftmost subspace is inconsistent since a different colored class prototype is preferred.

identify adversarial examples through an examination/manipulation of the inputs to DNNs [32, 54, 59].

- **Feature-space detection** - Methods which typically train new detector models on intermediate or final DNN layer outputs [39, 2, 9, 55, 13, 1, 40, 43, 49, 36, 12].
- **Robustness Certificates** - Theoretical proofs for DNN robustness under specific threat models (assumptions for both attacker and defender) [58, 47, 57, 56, 55, 51, 30, 33, 27, 28, 4, 15].
- **Statistical Detection** - Methods that focus on generating robust test statistics that separate clean from adversarial examples [31, 17, 46].
- **Network Coverage** - Methods that examine neuron coverage as a means to test DNN behavior and potentially establish differences between clean and adversarial examples [34, 35, 53, 52, 45].

Of specific relevance and similarity to our approach, are a set of high-performing methods [29, 36, 12, 43] which use local latent space geometry for AE detection. The work in [12] originally combined kernel density estimation and Bayesian uncertainty estimation to identify AEs as predicted-class outliers. Similarly, [29] examined detection through the lens of Gaussian Discriminant Analysis to estimate class confidence scores based on Mahalanobis distance (combined with a layer-wise logistic regression model to predict AE likelihood).

Both [36, 43] perform AE detection using nearest-neighbor principles where [36] relies on Local Intrinsic Dimensionality (LID) to characterize local neighborhood structure while [43] uses discrete k-Nearest Neighbors along with conformal prediction to identify neighborhood (in)consistencies. Our approach is inspired by elements of these papers and in particular, the approach towards AE detection by identifying (in)consistencies in latent-space behavior for both adversarial and clean examples.

3. Novel contributions

We present a novel approach to AE detection which leverages random projection subspace analysis to differentiate between model behavior under clean and adversarial conditions. Additional advantages and novel features of our proposed approach are as follows:

- Our detection scheme uses random projection subspaces to compare and analyze network activation behavior in a self-supervised manner.
- While most state of the art (SOTA) methods require some prior knowledge of attacks to train their detectors, our method is truly agnostic to attack strategy and goal, and requires a calibration set composed solely of clean examples.
- Additionally, while most detection methods rely on large calibration datasets, our method is extremely data efficient and requires only a fraction of the calibration data typically used. Our experiments show that calibration data requirements scale according to the number of classes rather than the method itself.
- Last, we evaluate our method under rigorous constraints by significantly reducing the size of the calibration set and restricting its composition to clean examples only (a true attack-agnostic paradigm). Under these more realistic and difficult conditions, our method far outperforms comparable methods across a variety of unseen attacks.

4. Background and Notation

We first provide some basic notation and assumptions. In typical image classification tasks, we start from a set of exemplars (x, y) where $x \in \mathbb{R}^{C \times W \times H}$ and $y \in Y = \{1, \dots, K\}$ (i.e., K classes). The aim is to produce a model, $f : X \rightarrow Y$, which minimizes a loss, $L(f(x; \theta), y)$. The

model is typically composed of a set of computational layers parameterized in aggregate by weight parameters θ giving us $\hat{y} = f(x; \theta)$. Assuming a purely feedforward model (a common form for image-based DNNs), we can decompose f as follows:

$$f(x; \theta) = f_L^{\theta_L} \circ f_{L-1}^{\theta_{L-1}} \circ \dots \circ f_2^{\theta_2} \circ f_1^{\theta_1}(x) = \hat{y} \quad (1)$$

where $f_l^{\theta_l}(\cdot) = z_l$

Note that for machine vision problems, $f(\cdot)$ is typically implemented as a deep neural network, whereby the intermediate layer activations, z_l may be 2D vectors or 3D tensors. Also, note that typically $f(\cdot)$ produces an output that represents a distribution over the N classes where $\hat{y} = \arg \max z_L$. During a forward pass of our model, we record and aggregate all intermediate activations into $z = \{z_1, \dots, z_L\}$.

5. Threat Model

We define an adversarial example as a perturbation, η , such that for a correctly classified clean input, $f(x; \theta) = \hat{y} = y_{true}$, whereas the added perturbation yields an incorrect classification, $f(x + \eta; \theta) = \hat{y} \neq y_{true}$. In targeted attacks cases, the AE is constructed to cause $\hat{y} = y_{target}$ whereas in untargeted scenarios, the AE is constructed to cause $\hat{y} \neq y_{true}$. In either case, the representation of the attacked image in feature space shifts away from its clean counterpart as illustrated in Figure 1.

In order to construct the most challenging detection task as possible from the perspective of the defender, we consider white-box scenarios whereby the attackers have full knowledge and access to the network weights and architecture to be attacked. In this setting, we assume that the attacker has access to the clean input and may modify it within specified constraints (e.g., a bound on the L_p -norm, i.e., $\|\eta\|_p \leq \epsilon$).

6. Adversarial Attack Detection Method

6.1. Dimensionality Reduction via Random Projections

Recent work by [22] provides evidence for the existence of *robust* and *non-robust but useful features* which contribute to task performance but crucially are informative regarding the susceptibility of the DNN to attacks. One possible mitigation strategy for adversarial manipulation of non-robust features is to perform dimensionality reduction of learned representations whereby the resulting features (from the *robust* set) preserve classification-relevant information and reduce or remove the impact of manipulated features (from the *non-robust* set).

Conventional dimensionality reduction techniques (e.g., Principal Components Analysis, Singular Value Decomposition, Independent Component Analysis) offer principled

approaches to achieving the reduction, but a primary disadvantage is that they are computationally expensive to compute in high-dimensions. Furthermore, while beneficial in many scenarios, these methods produce a single deterministic subspace which limits the scope for comparative analysis between properties of the reduced and full representations.

Instead, Random Projections (RP) do not have the aforementioned drawbacks, provide many desirable properties (explained later), and allow for more flexible analysis. Our approach will be to project layer activations into a series of random subspaces and then compare the relation of these reduced dimension projections with respect to class prototypes (in each subspace). Differences between clean and adversarial behavior will be exploited to produce the final detection. Definitions of these terms and details will be discussed in the following sections.

First, define a random projection of activation z_i as:

$$\hat{z}_i = Rz_i \quad (2)$$

where $R \in \mathbb{R}^{k \times d}$ ($k \ll d$), $z_i \in \mathbb{R}^d$, and $\hat{z}_i \in \mathbb{R}^k$, each R_{ij} is sampled independently from a standard normal distribution, and where representations are extracted from layer $i \in \{l \mid 1 \leq l \leq L\}$ of the DNN. Strictly speaking, the rows of R should be orthogonal. However, if R 's elements are sampled independently, it can be shown that the rows are approximately orthogonal ([3, 19]) and consequently the projections are reasonably approximate as well.

6.2. Theoretical Considerations

We draw particular motivation for using RP from the Johnson-Lindenstrauss Lemma which guarantees that with high probability, distances between pairs of points in the random subspace are preserved up to a scaling $(1 \pm \epsilon)$.

Lemma 6.1 (Johnson-Lindenstrauss [23])

Let $X = \{x_1, \dots, x_k\}$ in \mathbb{R}^n . There exists a random function $f: \mathbb{R}^n \rightarrow \mathbb{R}^m$ such that for any pair of points x_i, x_j

$$(1 - \epsilon) \|x_i - x_j\|_2^2 \leq \|f(x_i) - f(x_j)\|_2^2 \leq (1 + \epsilon) \|x_i - x_j\|_2^2 \quad (3)$$

with probability at least $\frac{1}{k}$ so long as $m \geq \frac{8 \log k}{\epsilon^2}$.

A proof of Lemma 6.1 can be found in [11].

The J-L Lemma is a statement about the existence of (random) embeddings in lower dimensions whereby the distortion of distances between a pair of points can be guaranteed to be bounded. This forms the basis for our detection method as it allows comparison between the proximity of points in the ambient feature space and in arbitrary random subspaces. Section 6.3 will describe how we can use random subspaces to check whether distances between suspected adversarial examples and known class prototypes re-

main consistent across random subspaces (with inconsistencies signalling a potential AE). The J-L Lemma guarantees that these distances should be preserved.

It is important to note that while the bound is tight, it represents a worst case scenario. In practice, distances are well-preserved below the theoretical value of m (see [3, 10]). Prior work has also reported that RP can help preserve other aspects of geometry such as cluster separability [10], volume, and distances to affine spaces [38], both theoretically and empirically. Connections between Restricted Isometry Property (RIP), a key ingredient for compressive sensing, and the J-L lemma were also made in [26].

6.3. Random Subspace Analysis

Our approach focuses on measuring the consistency of the local geometry around the test image embedding between the ambient and subspace representations. In particular, we leverage the ability to produce arbitrary random projections to compare DNN activations in multiple subspaces derived from the original full-dimensional space (illustrated conceptually in Figure 2).

More formally, define a set of M projections, $\{R_m | 1 \leq m \leq M\}$ applied to activation z_l from layer l to produce a set of subspace representations:

$$\hat{\mathbf{z}}_l = \{\hat{z}_{l,m}\} = \{R_m z_l | 1 \leq m \leq M\} \quad (4)$$

where elements of R_m are sampled independently from a standard normal distribution. When the random projection subspace is large, the projection vectors will tend to become normal to each other as the dimension increases. As shown in [3, 19], any sampling of R will be nearly orthonormal, ensuring that J-L Lemma holds in practice for arbitrary sampling using the standard normal distribution.

Because the RP preserves distances within some scaling, the potential loss of information can be advantageous. As evidenced by nearest-neighbor type analyses (e.g., [43]), adversarial features are likely to exhibit greater similarity to exemplars of the non-true class than the true class.

The existence of *robust* and *non-robust but useful features*, suggests that the non-robust features may be more likely than others to be manipulated under attack. Under a set of random projections, the influence of the manipulated features on the final outcome becomes increased/decreased as a function of the specific projection itself.

In the case that the manipulated features become less influential in the random subspace, the projection should show greater similarity to examples of the true class than the incorrect classes. Conversely, if the manipulated features become more influential, then the projection should show greater dissimilarity with the true class representation. When examined over a set of random projections, inconsistent behavior is more likely to be exposed and amplified.

For clean examples, projections should exhibit strong overall self-consistency to the true class across a set of projections (as suggested by the J-L lemma).

To build our detection model, we first extract layer-wise features z_l for each image x in a training dataset of clean images $\mathcal{D}_{\mathcal{T}} = \{(x, y) | x \in \mathbb{R}^{C \times W \times H}\}, y \in \{1, \dots, K\}$. We compute class-conditional prototypes:

$$\mu_{l,k} = \frac{1}{N_k} \sum_{i: y_i=k} f_l(x_i; \theta) \quad (5)$$

where N_k is the number of examples with class label k . Then, as described in Algorithm 1, we project both the test point features and the prototypes into the same subspace, determine the nearest prototype in the subspace, and return the associated label for each layer of interest.

Algorithm 1: Random Subspace Analysis

Result: Random Subspace Analysis
Input : z_l : Activation for the test image at layer l
 μ_l : Class prototypes (k) at layer l
 R_l : Set of M random projection matrices at layer l
 $d(\cdot)$: Distance function (i.e., euclidean, cosine)
Output: \mathcal{P}_l : Set of M predicted class labels (one per RP)

- 1 Initialize the RP nearest-label array $\mathcal{P}_l = []$;
- 2 **for** $m \in \{1, \dots, M\}$ **do**
- 3 Initialize distances array $D = []$;
- 4 Project activation: $\hat{z}_l = R_m z_l$;
- 5 **for** $k \in \{1, \dots, K\}$ **do**
- 6 Project prototype: $\hat{\mu}_{l,k} = R_m \mu_{l,k}$;
- 7 Add $d(\hat{z}_l, \hat{\mu}_{l,k})$ to D ;
- 8 Add $c = \arg \min_k(D)$ to \mathcal{P}_l ;
- 9 **return** \mathcal{P}_l ;

6.4. AE Detection

We next apply a simple decision rule on the nearest-prototype set \mathcal{P}_l (which contains the label of the nearest prototype to the test point in each subspace), to predict whether the test point is adversarial (represented as \hat{a}) and where $mode(\mathcal{P}_l)$ represents the label occurring most frequently in \mathcal{P}_l .

$$\hat{a} = \begin{cases} 1 & \text{if } \frac{1}{M} \sum_{c \in \mathcal{P}_l} \mathbb{1}(c = mode(\mathcal{P}_l)) < \alpha \text{ for } \alpha \in [0, 1] \\ 0 & \text{otherwise} \end{cases} \quad (6)$$

Note that the set \mathcal{P}_l may be replaced by \mathcal{P} which is simply an aggregation of label preference across multiple layers of the network (i.e., $\mathcal{P} = \bigcup \mathcal{P}_l$ for $l \in L' \subseteq L$). Essentially, Eq. 6 represents the fraction of label agreement across all

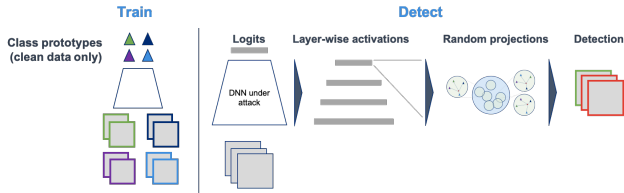


Figure 3. AE detection pipeline: Training: class prototypes are computed from clean data only (one prototype per class). Detection: activations computed for the test images (gray squares) are projected to a set of random subspaces and consistency is measured in terms of label preference.

random subspaces (as determined by the distance from the test point to its nearest prototype).

Of course, more powerful decision rules may be developed, but the rule in Eq. (6) provides several notable advantages: (1) it is interpretable and simple to compute, (2) it is tunable by a single hyperparameter α , (3) it is agnostic to the ground-truth label, and (4) it is non-differentiable (increasing its robustness against many powerful attacks). Note that $\alpha = 0$ corresponds to the degenerate case where x is always labeled as clean. In contrast, $\alpha = 1$ is the most stringent case such that the label for the nearest-prototype must be the same for all random projections in order for x to be considered clean. To be truly attack agnostic, the selection of α can be performed absent of any attack data (e.g., to reduce false alarms). However, if attack data is available, α may be tuned in a more principled way.

The benefit from (3) above is of particular importance given that the true class is not known for new test points, and thus we cannot condition the detection on the true label at inference. While many methods condition the detection on the DNN’s prediction \hat{y} (e.g., [43, 36, 12]), our approach considers only whether the label of the nearest prototype stays consistent across random subspaces. Thus, we are able to use class-level representations while still separating AE detection from image classification. In essence, our method takes advantage of competing elements of adversarial attacks, namely changing the predicted label of the model without changing the true meaning of the input.

7. Data and Models

7.1. Adversarial Example Generation

For evaluation purposes only, we generated sets of (*clean, adversarial*) image pairs on which to evaluate. We make use of the Foolbox toolkit [48] to generate attacks with varying complexity and strategy, including FGSM [16], PGD [37], CWL2 [7], JSMA [44], EAD [8], and gradient-free noise). We use the respective published attack hyperparameters during attack generation.

We evaluate our detection approach (Figure 3) under a white-box threat model whereby the adversary has full

knowledge of the network architecture and weights. Attack parameters are chosen to be consistent with those commonly found in the literature (which balance attack effectiveness and subtlety). This threat model provides an approximate lower-bound for detection given that the adversary should not be able to improve their attack under less-favorable conditions.

7.2. Data

For each experiment, we generate a set of 4000 (*clean, adversarial*) image pairs for each attack under consideration for CIFAR10, SVHN, and mini-ImageNet. To fit our detection model, we reserve 10% of the clean examples only for computing the class-specific prototypes and the remaining 90% of exemplars for evaluation.

For each attack, we follow standard practice for evaluating AE detection and evaluate only the (*clean, adversarial*) pairs where both elements achieve their objectives (i.e., correct classification, misclassification). In both cases, we avoid confounding our detector’s performance with other data/model-related issues that would come from misclassification of clean examples or failed attempts to attack the model.

7.3. White-box Models

We focus our efforts on attacking commonly used, high-performing architectures for image classification. We train ResNet[18,34] ([18]) and DenseNet161 ([21]) models from scratch on each dataset. We train for 200 epochs using SGD with a base learn rate of 10^{-1} (decreasing by 0.1 every 50 epochs starting from epoch 100), momentum of 0.9, and weight decay constant of 10^{-4} . These models are then used directly for the white-box attack generation to ensure the most challenging AE detection scenario.

7.4. Baselines and SOTA Comparisons

We evaluate our method against SOTA approaches from [29] and [36] which use local latent space geometry for adversarial detection. These methods are not attack agnostic, so we must modify these approaches to fit our paradigm. First, we are primarily interested in attack-agnostic detection so we must have detection methods that do not require any attack data during the detector calibration step. Second, we focus on a test paradigm where the calibration set is limited in size which emphasizes advantages of the method relative to any performance gained from more data. Modifying these baselines further allows better insight into whether the performance of those methods is attributed to the method itself or the access to ground truth attack data during training.

DMD-OC: The Deep Mahalanobis Detector (DMD) [29] applies Gaussian Discriminant Analysis to compute class-conditional confidence scores across a

set of DNN layers. The maximum score over all classes is taken at each layer and then a weighted sum of the scores is used to produce the final output. The original method trained a logistic regression classifier on clean and adversarial data using the confidence scores as features to learn an optimal weighting of layer-specific scores.

LID-OC: The Local Intrinsic Dimensionality (LID) [36] detector estimates the local intrinsic dimensionality of the test sample from its k -nearest neighbors (we use $k = 20$ as in the original paper) based on activations at selected layers in the DNN. Similar to DMD, the original method trained a logistic regression classifier on clean and AE data using the LID estimates across layers as features to predict if the test point is clean or adversarial.

For these baselines, in order to fit the attack-agnostic paradigm where adversarial data for training is not available, we replace the Logistic Regression classifiers in both methods with a One-Class Support Vector Machine (SVM) [50] trained only on clean activations. We do not modify the computation of the confidence scores or LID values, and we use the same DNN layers for all baseline detection methods.

8. Experiments

In all of the following experiments, we run our detection method using the output from the last layer prior to the classification layer. Following standard practice, the primary performance metric is ROC Area Under the Curve (AUC) score which allows us to sweep over decision thresholds (i.e., α for our method and similar for other baselines).

8.1. White-Box Attacks

We first consider AE detection for untargeted white-box attacks. Since our method is agnostic to the attack algorithm, we observe the detection performance across a range of attacks and consider the differences in performance between them. Table 1 illustrates the detection performance for untargeted attacks. In all cases, $k = 16$ for the RP dimension, $M = 8$ projections were used for the detector.

8.2. Sensitivity Studies

We run additional sensitivity studies to determine the impact of both the dimensionality of the random subspace as well as the number of subspaces considered during the detection process.

RP Dimension Dependency Table 2 shows the impact of changing the dimension of the RP on the AE detection result. In all cases, $M = 8$ projections were used for the layer prior to the final output layer. The full dimensionality of the final layer is 512, so the subspace dimensions studied here represent a modest-to-aggressive reduction.

Dependence on Number of Projections Table 3 captures the impact of the number of projections, M , consid-

ered at detection time. We fix the dimensionality to $k = 16$. We focus here on a range of projections to capture the trade-off between having sufficient data for measuring label consistency and over-inflating the computational requirements for performing detection.

Expanded Calibration Data We perform additional experiments which increase the amount of clean-only calibration data available to the detectors and present them in Table 4. Since the detectors are only fit to clean data and due to the limited size of the calibration/test splits for detection, we expand the available data by drawing from the original training set used for training the core model. While this is not common practice, this approach still has practical value since it allows the detectors to use prototypes based on embeddings the network was directly trained to produce. Data used for detection is held out as normal.

These results suggest that the strength of other detection methods scales in proportion to the available calibration data whereas our method provides consistent performance for small and larger training set sizes.

Targeted Attacks Table 6 captures the performance of the proposed method on targeted attacks. A target label was chosen at random from the CIFAR10 set and used to generate targeted attacks. The detector was calibrated on 20% of the clean samples. Results indicate that the proposed method significantly outperforms baselines even when the attack is steered towards a particular label.

8.3. Experiments on mini-ImageNet

We run additional experiments on mini-ImageNet to test the effectiveness of our method on more challenging data (Table 5). We focus on scaling the complexity of the detection task to the image data (higher resolution, greater diversity) rather than the classification task itself (e.g., more classes). For these experiments, we choose the DeepRP hyperparameters to be $M = 32$ and $k = 16$. We also expand the calibration dataset to be 2000 clean examples.

Results show that our method far outperforms all competing methods even as the images become more complex in terms of resolution and statistics. That said, we believe that the difficulty of the ImageNet data relative to CIFAR or SVHN motivates a greater expansion of the calibration dataset to get more stable estimates of the class prototypes.

9. Discussion

Experiments demonstrate the efficacy of our approach and leads to several key observations. First, the overall detection performance of our method is consistently high across attack algorithms, demonstrating a degree of independence between our detection method and the details of the attack (under the same threat model). Slight differences occur between the detection performance given the archi-

Table 1. AUC score for detection of white-box untargeted perturbation attacks on CIFAR10 and SVHN. Best methods indicated in **bold**.

Dataset	Architecture	Detector	Attack					
			FGSM	PGD	JSMA	EAD	CWL2	Noise
CIFAR10	ResNet18	LID-OC	0.570	0.525	0.547	0.509	0.540	0.533
		DeepMD-OC	0.502	0.550	0.547	0.547	0.551	0.553
		DeepRP (ours)	0.955	0.964	0.962	0.951	0.954	0.930
	ResNet34	LID-OC	0.495	0.522	0.519	0.512	0.498	0.505
		DeepMD-OC	0.500	0.601	0.594	0.585	0.583	0.602
		DeepRP (ours)	0.946	0.974	0.972	0.941	0.966	0.915
	DenseNet161	LID-OC	0.491	0.496	0.533	0.493	0.486	0.553
		DeepMD-OC	0.500	0.500	0.500	0.500	0.500	0.500
		DeepRP (ours)	0.928	0.926	0.931	0.920	0.926	0.952
SVHN	ResNet18	LID-OC	0.601	0.482	0.480	0.487	0.468	0.299
		DeepMD-OC	0.501	0.603	0.569	0.603	0.584	0.571
		DeepRP (ours)	0.954	0.957	0.965	0.951	0.952	0.950
	ResNet34	LID-OC	0.543	0.509	0.514	0.494	0.475	0.384
		DeepMD-OC	0.507	0.591	0.580	0.595	0.592	0.577
		DeepRP (ours)	0.953	0.937	0.956	0.944	0.944	0.923
	DenseNet161	LID-OC	0.513	0.581	0.585	0.588	0.569	0.795
		DeepMD-OC	0.500	0.500	0.500	0.500	0.500	0.500
		DeepRP (ours)	0.959	0.972	0.975	0.967	0.967	0.968

ture under attack, but the detection performance is consistent.

Our method also outperforms the other baselines given limited access to clean-only training data. This performance difference is mostly attributed to the significant reduction in the calibration set size. While all methods benefit greatly from having more calibration data (i.e., to produce more stable prototypes (ours), reduce the sparsity of the latent space (LID), improve the mean/covariance estimates (DMD)), results indicate that our approach is considerably more robust under this constraint. This lends credence to the use of our approach under a greater range of conditions where the attack is unknown and available calibration data may be limited.

Tables 2 and 3 indicate some dependence on both the dimension of the random projection (k) and the number of projections considered during the detection process (M). There is a clear tradeoff between choices of k and M . For k , results suggest that the RP must perform a certain degree of representation compression, but too little compression results in a representation too similar to the original (i.e., inclusion of too many non-robust features) and too much results in a significant loss of information (i.e., loss of robust *and* non-robust features). For M , the balance must be between too few subspaces under consideration (i.e., resulting in insufficient observations of activation behavior) and too many (i.e., where subspace diversity becomes less prominent).

Furthermore, the additive noise attack produces, in general, the lowest detection performance. Since this attack requires no knowledge of the underlying model architecture or weights, it is unable to preferentially target (implicitly or explicitly) the non-robust features over the robust ones. As such, the random subspaces are more likely to produce consistent behavior and thereby miss possible

detections. While this attack is notably weak compared to more sophisticated approaches (e.g.,[7]), it highlights how an adaptive adversary might attempt to circumvent our detection scheme. However, while modifying an attack to more evenly manipulate features may evade detection, it may have unintended and detrimental consequences on the overall viability of the attack itself. We leave it to future work to investigate this tradespace of competing objectives in more depth.

Lastly, recent literature [5, 20, 14, 42] has provided new methods for detecting out-of-distribution or anomalous samples wherein adversarial examples may be viewed as a special case. Specifically, recent and concurrently developed self-supervised [41] and unsupervised [24, 25] methods in those problem domains present a promising direction for future research.

10. Conclusions

We present a novel approach to adversarial example detection via random subspace analysis. We use random projections to reduce dimensionality of deep features and then examine the consistency of features across a set of subspaces to detect attacks. We evaluate our method under much more rigorous constraints than prior approaches by constraining the calibration set to clean examples only.

Our results demonstrate that our approach, while being agnostic to the attack strategy or objective (i.e., targeted/untargeted), consistently outperforms against a range of SOTA attack strategies with various degrees of sophistication. We believe that this work opens up new approaches for analyzing deep features in the context of adversarial example detection via random subspace analysis.

Table 2. AUC score for detection of white-box untargeted perturbation attacks on CIFAR10, SVHN as the dimension of the RP changes. Best results indicated in **bold face**.

Dataset	Architecture	Detector	Attack					
			FGSM	PGD	JSMA	EAD	CWL2	Noise
CIFAR10	ResNet18	DeepRP-k8	0.935	0.948	0.947	0.940	0.928	0.948
		DeepRP-k16	0.955	0.964	0.962	0.951	0.954	0.930
		DeepRP-k32	0.961	0.959	0.961	0.943	0.945	0.901
		DeepRP-k64	0.952	0.958	0.945	0.926	0.931	0.843
		DeepRP-k128	0.910	0.918	0.904	0.855	0.873	0.752
SVHN	ResNet18	DeepRP-k8	0.953	0.958	0.966	0.961	0.959	0.967
		DeepRP-k16	0.954	0.957	0.965	0.951	0.952	0.950
		DeepRP-k32	0.934	0.916	0.943	0.909	0.922	0.904
		DeepRP-k64	0.877	0.845	0.879	0.838	0.848	0.834
		DeepRP-k128	0.824	0.779	0.811	0.775	0.783	0.768

Table 3. AUC score for detection of white-box untargeted perturbation attacks on CIFAR10, SVHN as the number of projections changes. Best results indicated in **bold face**.

Dataset	Architecture	Detector	Attack					
			FGSM	PGD	JSMA	EAD	CWL2	Noise
CIFAR10	ResNet18	DeepRP-M2	0.768	0.770	0.771	0.750	0.764	0.786
		DeepRP-M4	0.895	0.911	0.910	0.889	0.904	0.891
		DeepRP-M8	0.955	0.964	0.962	0.951	0.954	0.930
		DeepRP-M16	0.968	0.976	0.974	0.966	0.965	0.953
		DeepRP-M32	0.974	0.980	0.980	0.971	0.970	0.966
SVHN	ResNet18	DeepRP-M2	0.767	0.753	0.770	0.761	0.767	0.823
		DeepRP-M4	0.904	0.901	0.920	0.894	0.895	0.910
		DeepRP-M8	0.954	0.957	0.965	0.951	0.952	0.950
		DeepRP-M16	0.966	0.972	0.974	0.964	0.967	0.960
		DeepRP-M32	0.970	0.977	0.979	0.972	0.976	0.971

Table 4. AUC score for detection of white-box untargeted perturbation attacks on CIFAR10 for 10x more training data. Best methods indicated in **bold face**.

Dataset	Architecture	Detector	Attack					
			FGSM	PGD	JSMA	CWL2	Noise	
CIFAR10	ResNet18	LID-OC	0.495	0.525	0.525	0.535	0.763	
		DeepMD-OC	0.833	0.864	0.885	0.860	0.849	
		DeepRP (ours)	0.961	0.966	0.963	0.957	0.948	
	ResNet34	LID-OC	0.486	0.493	0.584	0.556	0.739	
		DeepMD-OC	0.837	0.899	0.904	0.902	0.861	
		DeepRP (ours)	0.965	0.973	0.971	0.967	0.928	

Table 5. AUC score for detection of white-box untargeted perturbation attacks on mini-Imagenet for 2k clean examples for training. Best methods indicated in **bold face**.

Dataset	Architecture	Detector	Attack					
			FGSM	PGD	JSMA	EAD	CWL2	Noise
mini-ImageNet	ResNet18	LID-OC	0.533	0.537	0.502	0.524	0.528	0.498
		DeepMD-OC	0.449	0.472	0.476	0.470	0.464	0.558
		DeepRP (ours)	0.790	0.760	0.749	0.744	0.760	0.871

Table 6. AUC score for detection of white-box targeted perturbation attacks on CIFAR10. Best methods indicated in **bold face**.

Dataset	Architecture	Detector	Attack			
			FGSM	PGD	JSMA	CWL2
CIFAR10	ResNet18	LID-OC	0.365	0.475	0.525	0.513
		DeepMD-OC	0.500	0.618	0.655	0.614
		DeepRP	0.517	0.858	0.872	0.878
	ResNet34	LID-OC	0.532	0.511	0.497	0.515
		DeepMD-OC	0.500	0.563	0.571	0.577
		DeepRP	0.528	0.870	0.885	0.871

References

- [1] Tarek Abdelzaher, Nora Ayanian, Tamer Basar, Suhas Digavi, Jana Diesner, Deepak Ganesan, Ramesh Govindan, Susmit Jha, Tancrede Lepoint, Benjamin Marlin, et al. Toward an internet of battlefield things: A resilience perspective. *Computer*, 51(11):24–36, 2018.
- [2] Alexander Bagnall, Razvan Bunescu, and Gordon Stewart. Training ensembles to detect adversarial examples. *arXiv preprint arXiv:1712.04006*, 2017.
- [3] Ella Bingham and Heikki Mannila. Random projection in dimensionality reduction: applications to image and text data. In *Proceedings of the seventh ACM SIGKDD international conference on Knowledge discovery and data mining*, pages 245–250, 2001.
- [4] Akhilan Boopathy, Tsui-Wei Weng, Pin-Yu Chen, Sijia Liu, and Luca Daniel. Cnn-cert: An efficient framework for certifying robustness of convolutional neural networks. In *Proceedings of the AAAI Conference on Artificial Intelligence*, volume 33, pages 3240–3247, 2019.
- [5] Saikiran Bulusu, Bhavya Kaikhura, Bo Li, Pramod K Varshney, and Dawn Song. Anomalous example detection in deep learning: A survey. *IEEE Access*, 8:132330–132347, 2020.
- [6] Nicholas Carlini and David Wagner. Adversarial examples are not easily detected: Bypassing ten detection methods. In *Proceedings of the 10th ACM Workshop on Artificial Intelligence and Security*, pages 3–14, 2017.
- [7] Nicholas Carlini and David Wagner. Towards evaluating the robustness of neural networks. In *2017 IEEE Symposium on Security and Privacy (SP)*, pages 39–57. IEEE, 2017.
- [8] Pin-Yu Chen, Yash Sharma, Huan Zhang, Jinfeng Yi, and Cho-Jui Hsieh. Ead: elastic-net attacks to deep neural networks via adversarial examples. *arXiv preprint arXiv:1709.04114*, 2017.
- [9] F Crecchi, D Bacciu, and B Biggio. Detecting adversarial examples through nonlinear dimensionality reduction. In *27th European Symposium on Artificial Neural Networks, Computational Intelligence and Machine Learning, ESANN 2019*, pages 483–488. ESANN (i6doc. com), 2019.
- [10] Sanjoy Dasgupta. Experiments with random projection. *arXiv preprint arXiv:1301.3849*, 2013.
- [11] Sanjoy Dasgupta and Anupam Gupta. An elementary proof of the johnson-lindenstrauss lemma. *International Computer Science Institute, Technical Report*, 22(1):1–5, 1999.
- [12] Reuben Feinman, Ryan R Curtin, Saurabh Shintre, and Andrew B Gardner. Detecting adversarial samples from artifacts. *arXiv preprint arXiv:1703.00410*, 2017.
- [13] Gil Fidel, Ron Bitton, and Asaf Shabtai. When explainability meets adversarial learning: Detecting adversarial examples using shap signatures. *arXiv preprint arXiv:1909.03418*, 2019.
- [14] Stanislav Fort, Jie Ren, and Balaji Lakshminarayanan. Exploring the limits of out-of-distribution detection. *arXiv preprint arXiv:2106.03004*, 2021.
- [15] Timon Gehr, Matthew Mirman, Dana Drachslor-Cohen, Petar Tsankov, Swarat Chaudhuri, and Martin Vechev. Ai2: Safety and robustness certification of neural networks with abstract interpretation. In *2018 IEEE Symposium on Security and Privacy (SP)*, pages 3–18. IEEE, 2018.
- [16] Ian J Goodfellow, Jonathon Shlens, and Christian Szegedy. Explaining and harnessing adversarial examples. *arXiv preprint arXiv:1412.6572*, 2014.
- [17] Kathrin Grosse, Praveen Manoharan, Nicolas Papernot, Michael Backes, and Patrick McDaniel. On the (statistical) detection of adversarial examples. *arXiv preprint arXiv:1702.06280*, 2017.
- [18] Kaiming He, Xiangyu Zhang, Shaoqing Ren, and Jian Sun. Deep residual learning for image recognition. In *Proceedings of the IEEE conference on computer vision and pattern recognition*, pages 770–778, 2016.
- [19] Robert Hecht-Nielsen et al. Context vectors: general purpose approximate meaning representations self-organized from raw data. *Computational intelligence: Imitating life*, 3(11):43–56, 1994.
- [20] Yen-Chang Hsu, Yilin Shen, Hongxia Jin, and Zsolt Kira. Generalized odin: Detecting out-of-distribution image without learning from out-of-distribution data. In *Proceedings of the IEEE/CVF Conference on Computer Vision and Pattern Recognition*, pages 10951–10960, 2020.
- [21] Gao Huang, Zhuang Liu, Laurens Van Der Maaten, and Kilian Q Weinberger. Densely connected convolutional networks. In *Proceedings of the IEEE conference on computer vision and pattern recognition*, pages 4700–4708, 2017.
- [22] Andrew Ilyas, Shibani Santurkar, Dimitris Tsipras, Logan Engstrom, Brandon Tran, and Aleksander Madry. Adversarial examples are not bugs, they are features. In *Advances in Neural Information Processing Systems*, pages 125–136, 2019.
- [23] William B Johnson and Joram Lindenstrauss. Extensions of lipschitz mappings into a hilbert space. *Contemporary mathematics*, 26(189-206):1, 1984.
- [24] Gihyuk Ko and Gyumin Lim. Unsupervised detection of adversarial examples with model explanations. *arXiv preprint arXiv:2107.10480*, 2021.
- [25] Rajat Koner, Poulami Sinhamahapatra, Karsten Roscher, Stephan Günnemann, and Volker Tresp. Oodformer: Out-of-distribution detection transformer. *arXiv preprint arXiv:2107.08976*, 2021.
- [26] Felix Kraemer and Rachel Ward. New and improved johnson–lindenstrauss embeddings via the restricted isometry property. *SIAM Journal on Mathematical Analysis*, 43(3):1269–1281, 2011.
- [27] Aounon Kumar, Alexander Levine, Tom Goldstein, and Soheil Feizi. Curse of dimensionality on randomized smoothing for certifiable robustness. *arXiv preprint arXiv:2002.03239*, 2020.
- [28] Mathias Lecuyer, Vaggelis Atlidakis, Roxana Geambasu, Daniel Hsu, and Suman Jana. Certified robustness to adversarial examples with differential privacy. In *2019 IEEE Symposium on Security and Privacy (SP)*, pages 656–672. IEEE, 2019.
- [29] Kimin Lee, Kibok Lee, Honglak Lee, and Jinwoo Shin. A simple unified framework for detecting out-of-distribution samples and adversarial attacks. In *Advances in Neural Information Processing Systems*, pages 7167–7177, 2018.

- [30] Alexander Levine and Soheil Feizi. Wasserstein smoothing: Certified robustness against wasserstein adversarial attacks. *arXiv preprint arXiv:1910.10783*, 2019.
- [31] Xin Li and Fuxin Li. Adversarial examples detection in deep networks with convolutional filter statistics. In *Proceedings of the IEEE International Conference on Computer Vision*, pages 5764–5772, 2017.
- [32] Bin Liang, Hongcheng Li, Miaoqiang Su, Xirong Li, Wenchang Shi, and Xiaofeng Wang. Detecting adversarial image examples in deep neural networks with adaptive noise reduction. *IEEE Transactions on Dependable and Secure Computing*, 2018.
- [33] Zhaoyang Lyu, Ching-Yun Ko, Zhifeng Kong, Ngai Wong, Dahua Lin, and Luca Daniel. Fastened crown: Tightened neural network robustness certificates. *arXiv preprint arXiv:1912.00574*, 2019.
- [34] Lei Ma, Felix Juefei-Xu, Fuyuan Zhang, Jiyuan Sun, Minhui Xue, Bo Li, Chunyang Chen, Ting Su, Li Li, Yang Liu, et al. Deepgauge: Multi-granularity testing criteria for deep learning systems. In *Proceedings of the 33rd ACM/IEEE International Conference on Automated Software Engineering*, pages 120–131, 2018.
- [35] Lei Ma, Fuyuan Zhang, Minhui Xue, Bo Li, Yang Liu, Jianjun Zhao, and Yadong Wang. Combinatorial testing for deep learning systems. *arXiv preprint arXiv:1806.07723*, 2018.
- [36] Xingjun Ma, Bo Li, Yisen Wang, Sarah M Erfani, Sudanthi Wijewickrema, Grant Schoenebeck, Dawn Song, Michael E Houle, and James Bailey. Characterizing adversarial subspaces using local intrinsic dimensionality. *arXiv preprint arXiv:1801.02613*, 2018.
- [37] Aleksander Madry, Aleksandar Makelov, Ludwig Schmidt, Dimitris Tsipras, and Adrian Vladu. Towards deep learning models resistant to adversarial attacks. *arXiv preprint arXiv:1706.06083*, 2017.
- [38] Avner Magen. Dimensionality reductions that preserve volumes and distance to affine spaces, and their algorithmic applications. In *International Workshop on Randomization and Approximation Techniques in Computer Science*, pages 239–253. Springer, 2002.
- [39] Jan Hendrik Metzen, Tim Genewein, Volker Fischer, and Bastian Bischoff. On detecting adversarial perturbations. *arXiv preprint arXiv:1702.04267*, 2017.
- [40] David J Miller, Yulia Wang, and George Kesidis. When not to classify: Anomaly detection of attacks (ada) on dnn classifiers at test time. *arXiv preprint arXiv:1712.06646*, 2017.
- [41] Sina Mohseni, Mandar Pitale, JBS Yadawa, and Zhangyang Wang. Self-supervised learning for generalizable out-of-distribution detection. In *Proceedings of the AAAI Conference on Artificial Intelligence*, volume 34, pages 5216–5223, 2020.
- [42] Ibrahima Ndiour, Nilesh Ahuja, and Omesh Tickoo. Out-of-distribution detection with subspace techniques and probabilistic modeling of features. *arXiv preprint arXiv:2012.04250*, 2020.
- [43] Nicolas Papernot and Patrick McDaniel. Deep k-nearest neighbors: Towards confident, interpretable and robust deep learning. *arXiv preprint arXiv:1803.04765*, 2018.
- [44] Nicolas Papernot, Patrick McDaniel, Somesh Jha, Matt Fredrikson, Z Berkay Celik, and Ananthram Swami. The limitations of deep learning in adversarial settings. In *2016 IEEE European symposium on security and privacy (EuroS&P)*, pages 372–387. IEEE, 2016.
- [45] Kexin Pei, Yinzhi Cao, Junfeng Yang, and Suman Jana. Deepxplore: Automated whitebox testing of deep learning systems. In *proceedings of the 26th Symposium on Operating Systems Principles*, pages 1–18, 2017.
- [46] Igor M Quintanilha, Roberto de ME Filho, José Lezama, Mauricio Delbracio, and Leonardo O Nunes. Detecting out-of-distribution samples using low-order deep features statistics. 2018.
- [47] Aditi Raghunathan, Jacob Steinhardt, and Percy Liang. Certified defenses against adversarial examples. *arXiv preprint arXiv:1801.09344*, 2018.
- [48] Jonas Rauber, Wieland Brendel, and Matthias Bethge. Foolbox: A python toolbox to benchmark the robustness of machine learning models. *arXiv preprint arXiv:1707.04131*, 2017.
- [49] Kevin Roth, Yannic Kilcher, and Thomas Hofmann. The odds are odd: A statistical test for detecting adversarial examples. In *International Conference on Machine Learning*, pages 5498–5507, 2019.
- [50] Bernhard Schölkopf, John C Platt, John Shawe-Taylor, Alex J Smola, and Robert C Williamson. Estimating the support of a high-dimensional distribution. *Neural computation*, 13(7):1443–1471, 2001.
- [51] Sahil Singla and Soheil Feizi. Robustness certificates against adversarial examples for relu networks. *arXiv preprint arXiv:1902.01235*, 2019.
- [52] Youcheng Sun, Xiaowei Huang, Daniel Kroening, James Sharp, Matthew Hill, and Rob Ashmore. Testing deep neural networks. *arXiv preprint arXiv:1803.04792*, 2018.
- [53] Youcheng Sun, Min Wu, Wenjie Ruan, Xiaowei Huang, Marta Kwiatkowska, and Daniel Kroening. Concolic testing for deep neural networks. In *Proceedings of the 33rd ACM/IEEE International Conference on Automated Software Engineering*, pages 109–119, 2018.
- [54] Shixin Tian, Guolei Yang, and Ying Cai. Detecting adversarial examples through image transformation. In *Thirty-Second AAAI Conference on Artificial Intelligence*, 2018.
- [55] Lu Wang, Xuanqing Liu, Jinfeng Yi, Zhi-Hua Zhou, and Cho-Jui Hsieh. Evaluating the robustness of nearest neighbor classifiers: A primal-dual perspective. *arXiv preprint arXiv:1906.03972*, 2019.
- [56] Lily Weng, Pin-Yu Chen, Lam Nguyen, Mark Squillante, Akhilan Boopathy, Ivan Oseledets, and Luca Daniel. Proven: Verifying robustness of neural networks with a probabilistic approach. In *International Conference on Machine Learning*, pages 6727–6736, 2019.
- [57] Lily Weng, Huan Zhang, Hongge Chen, Zhao Song, Cho-Jui Hsieh, Luca Daniel, Duane Boning, and Inderjit Dhillon. Towards fast computation of certified robustness for relu networks. In *International Conference on Machine Learning*, pages 5276–5285, 2018.
- [58] Eric Wong and Zico Kolter. Provable defenses against adversarial examples via the convex outer adversarial polytope.

In *International Conference on Machine Learning*, pages 5286–5295, 2018.

- [59] Weilin Xu, David Evans, and Yanjun Qi. Feature squeezing: Detecting adversarial examples in deep neural networks. *arXiv preprint arXiv:1704.01155*, 2017.